Efficient removal of estrogenic compounds in water by MnIII-activated peroxymonosulfate: Mechanisms and application in sewage treatment plant water

Daqing Jia, Qinzhi Li, Khalil Hanna, Gilles Mailhot, Marcello Brigante

Efficient removal of estrogenic compounds in water by Mn^{III}-activated peroxymonosulfate: mechanisms and application in sewage treatment plant water

Daqing Jia[1], Qinzhi Li[2], Khalil Hanna[2,3], Gilles Mailhot[1], Marcello Brigante[1*]

[1] Université Clermont Auvergne, CNRS, Clermont Auvergne INP SIGMA Clermont, Institut de Chimie de Clermont-Ferrand, F-63000 Clermont-Ferrand, France.

[2] Univ. Rennes, École Nationale Supérieure de Chimie de Rennes, CNRS, ISCR – UMR6226, F-35000 Rennes, France

[3] Institut Universitaire de France (IUF), MESRI, 1 rue Descartes, 75231 Paris, France.

* Corresponding author: Marcello Brigante
E-mail: marcello.brigante@uca.fr
Tel : +33-0473405514

Abstract

In this paper, the degradation of three endocrine-disrupting chemicals (EDCs): bisphenol A (BPA), 17β-estradiol (E2) and 17α-ethinylestradiol (EE2) by manganite (γ-MnOOH) activated peroxymonosulfate (PMS) was investigated. Preliminary optimisation experiments showed that complete degradation of the three EDCs was achieved after 30 min of reaction using 0.1 g L^{-1} of γ-MnOOH and 2 mM of PMS. The degradation rate constants were determined to be 0.20, 0.22 and 0.15 min^{-1} for BPA, E2 and EE2, respectively. Combining radical scavenging approaches, Electron paramagnetic resonance (EPR) and X-ray photoelectron spectroscopy (XPS) analyses, we revealed for the first time that about 40 % of EDCs degradation can be attributed to heterogeneous electron transfer reaction involving freshly generated Mn(IV), and 60 % to sulfate radical degradation pathway. The influence of various inorganic ions on the γ-MnOOH/PMS system indicated that removal efficiency was slightly affected by chloride and carbonate ions, while nitrate and nitrite ions had negligible impacts. The application of γ-MnOOH/PMS system in real sewage treatment plant water (STPW) showed that degradation rate constants of EDCs decreased to 0.035-0.048 min^{-1} and complete degradation of the three EDCs after 45 min. This study provides new insights into the reactivity of combined γ-MnOOH and PMS, and opens new ways for the application of Mn-bearing species in wastewater treatment technologies.

Keywords: Manganite; Peroxymonosulfate; Metal-based oxidation; Sulfate radical; EDCs

1. Introduction

Endocrine-disrupting chemicals (EDCs) affect the normal functioning of endogenous hormones (Zhou et al., 2019). EDCs consist of various types of chemicals such as natural and synthetic hormones, plasticizers, pesticides, and flame retardants (C. Yang et al., 2020). With the development of industry and the pursuit of high-quality life of humans, the EDCs-containing products have been consumed in a large amount. Over the past 10 years, EDCs as a major concern of water quality have received extensive attention (Adeel et al., 2017; Havens et al., 2020; Vilela et al., 2018). The regularly detected amount of EDCs in surface and drinking waters are up to ng/L while higher concentrations in municipal wastewater, an important source of anthropogenic pollution release into the environment, were also reported (Adeel et al., 2017; Lei et al., 2020).

To decrease the concentration of EDCs in wastewater, different processes based on thermal and photochemical degradation were reported (Chaves et al., 2020; Gabet et al., 2021; Gmurek et al., 2017). Advanced oxidation processes (AOPs) are innovative technologies used to improve the degradation of the recalcitrant pollutants based on the formation of highly oxidative species (Gabet et al., 2021; Gmurek et al., 2017). Reactive oxygen and sulfur species (ROS and RSS) with high oxidation potentials such as hydroxyl ($HO^{\bullet}$) and sulfate ($SO_4^{\bullet-}$) radicals are generated through photochemical or electron transfer reaction (Gligorovski et al., 2015). Such radicals are capable of inducing hazardous pollutants degradation till complete mineralization in water. Among the different AOPs systems, transition metal-based activation of radical precursors represents a low-energy cost and efficient process (Wang and Wang, 2018; Xiong et al., 2020). Iron (Fe) is one of the most used metal in homogeneous and heterogeneous applications and the redox cycle between Fe(II) and Fe(III) provide a very efficient system for activation of radical precursors and abatement of organic pollutant concentration in waters (Kusic et al., 2011).

However, organic complexes such as aminopolycarboxylic are regularly used to improve the iron stability toward a large range of pH values (Abida et al., 2006; Huang et al., 2013).

Recently, other metals such as manganese (Mn) has been used for different water treatment applications. Mn is a promising metal due to its multiple oxidation states (+II, +III, +IV, +VII) and high oxidative and catalytic reactivity. Most of published reports have focused on manganese dioxide–based AOPs (MnO_2-AOPs), to remove pollutants, such as phenol and 2,4–dichlorophenol, using MnO_2 activated peroxymonosulfate (PMS) or persulfate (PS) in water (Wang et al., 2015; Zhao et al., 2016). Huang et al. (2019) investigated the effects of properties of MnO_2 such as crystal structure, morphology, and surface Mn oxidation states on PMS activation. They showed that the catalytic activity of MnO_2 is positively corrected with the surface Mn(III) content (Huang et al., 2019).

Other studies have used Mn(III) oxides as a mean to activate oxidants (e.g. PMS and PS) and then remove organic contaminants, such as α-Mn_2O_3 (Saputra et al., 2014) and MnOOH (Xu et al., 2021). He et al. demonstrated that nanowires MnOOH have higher activity on PMS activation for 2,4-dichlorophenol oxidation as compared with multi-branches and nanorods MnOOH (He et al., 2020). Moreover, (Li et al., 2016) showed that sulfate and hydroxyl radicals can be generated from manganite-activated PS under pH 11. Although the good ability of Mn^{III}-oxides for PS or PMS activation has been investigated the underlying mechanisms of activation and generation of reactive species remain elusive. In addition, most of available data on the MnOOH/PMS activation process has been obtained in ultrapure water and very little is known about the application of this process in real wastewater. Therefore, the ability of γ-MnOOH for PMS activation under real-world conditions for wastewater treatment merits investigation.

In the present study, we investigated the degradation of three EDCs (Bisphenol A (BPA), 17β-estradiol (E2) and 17α-ethinylestradiol (EE2)) using γ-MnOOH-activated PMS process. We

have combined radical scavenging approaches, EPR and XPS analyses, to determine the different activation and removal mechanisms (i.e. radical and non-radical pathways). Moreover, the influence of key parameters such as the initial concentration of γ-MnOOH and PMS, and the impact of water inorganic constituents were also evaluated. Finally, the efficiency of the degradation system was evaluated in real sewage treatment plant water, collected from the "3 rivières" urban treatment plant in Clermont-Ferrand, France.

2. Material and Methods

2.1. Chemicals and reagents

Bisphenol A (BPA, 99%), 17β-estradiol (E2, 98%), 17α-ethynylestradiol (EE2, 98%), potassium peroxymonosulfate (PMS, purchased in the form of $KHSO_5 \cdot 0.5KHSO_4 \cdot 0.5K_2SO_4$), sodium nitrite ($NaNO_2$, 97%), sodium bicarbonate ($NaHCO_3$, 99.7%), and sodium chloride (NaCl, 99%) were purchased from Sigma-Aldrich Company, France. Sodium nitrate ($NaNO_3$, 99%) was bought from Fluka. Manganese (II) chloride ($MnCl_2$) was purchased from Riedel-de Haen. HPLC grade acetonitrile solvent (ACN) was purchased from CARLO ERBA Reagents. Sodium hydroxide (NaOH, 99.9%) and perchloric acid ($HClO_4$, 72%) which were used to adjust solution pH were purchased from Sigma-Aldrich. Ethanol (96%, VWR Chemicals), *t*-Butyl alcohol (TBA), and furfuryl alcohol (FFA) from Sigma-Aldrich were employed as radical and singlet oxygen scavengers. Ultrapure water (Millipore, resistivity 18.2 MΩ cm) was used in the preparation of all solutions. All chemicals were used as received without further purification.

2.2. γ-MnOOH synthesis and characterization

Manganite (γ-MnOOH) particles were synthesized as described by Yu and co-workers (Yu et al., 2018). The nature of γ-MnOOH was confirmed by X-ray diffraction (XRD) and

Transmission Electron Microscopy- Selective Area Electron Diffraction (TEM-SAED) using an accelerating voltage of 200 kV (TEM Jeol JEM 2100 HR) (Fig. S1). TEM images of the as-prepared manganite display wire-like morphology with diameters of 20–40 nm, and the SAED pattern confirmed the nature of γ-MnOOH. For XPS analysis, 0.5 g/L of solid were put in contact with 5 mM of PMS with and without BPA (200 µM). After 1 h of reaction, the solution was centrifuged and water was withdrawn and the remaining water completely removed under the N_2 stream. Then, the solid particles were collected and analyzed in a UHV chamber (pressure 10^{-7} Pa) facilitated with an XPS system (hemispherical electron energy analyzer OMICRON EA125, Germany). Data analysis, curve fitting and quantification of the Mn XPS spectra were performed using CasaXPS software. The binding energy (BE) scale was referenced to the adventitious C1s peak at 284.8 eV. High-resolution XPS spectra were processed using Shirley background subtraction. After background subtraction, the spectra were smoothed and fitted by using of Gaussian-Lorentzian peak shape (70:30). For each sample, fitting parameters (FWHM, the full width at half maximum; H, the peak height; E, the peak position center) were adjusted to minimize the value of residual standard deviation (STD).

2.3. Real water matrix

The sewage treatment plant water (STPW) was collected from the urban treatment plant named "3 rivières" in Clermont-Ferrand, France in December 2019. Prior to use, the STP water was filtered using a syringe filter (CHROMAFIL® Xtra RC-45/25) and then use for experiments. The main physico-chemical parameters relevant to this study are reported in Table S1.

2.4. Experimental procedure

PMS was added to the solution containing selected EDCs and γ–MnOOH just before the reaction starts. All reactions were performed in a brown glass bottle (125 mL) at room

temperature (293 ± 2 K) and under stirring to ensure homogeneity. Unless otherwise stated, experiments were performed at pH 6.5 ± 0.2. For HPLC, 2 mL of solution were withdrawn at fixed interval times, filtered using 0.20 µM PTFE filter and the reaction was immediately quenched with the addition of 20% methanol (HPLC grade, Sigma-Aldrich). Samples were kept at 277 K and analysis was performed within 4 hours. Furthermore, to identify the generated radicals, EtOH, TBA and FFA were added to the solution before PMS addition and a kinetic approach based on the second-order rate constants and pseudo-first order decay determination was used to assess the radical species involvement.

2.5. Analytical methods

BPA, E2 and EE2 quantification during reactions was performed by high performance liquid chromatography (HPLC) equipped with a diode array detector (Waters 2475, USA). The injection volume was 50 µL and a flow rate of 1 mL min^{-1} with a mobile phase consisting of a mixture of water and ACN (50/50, v/v) were used. An Agilent Eclipse XDB C18 of 250 mm × 4.6 mm × 5 µm column was adapted as the analytic column. Under these conditions, the detection wavelength and retention time were: for BPA (277 nm) at 5.4 min, for E2 (280 nm) at 6.2 min, for EE2 (280 nm) at 7.3 min (Fig. S2). To investigate the mineralization, the total organic carbon (TOC) analysis (TOC-L CPH CN200, Shimadzu) was performed.

The pseudo-first order decay of selected pollutant (k'_p) was determined from the slope of $\ln(C/C_0)$ *vs* reaction time as following: $ln\frac{C}{C_0} = k'_p \times t$. Where C_0 and C are the initial and remaining concentrations in solution and *t* is the reaction time.

PMS was quantified using the iodometric titration in which generated I_3^- was quantified at 348 nm using a Cary 300 Varian Spectrophotometer (Wacławek et al., 2015). Calibration was performed using different PMS concentrations and data are presented in the supplementary Materials (Fig. S3). Briefly, 100 µL of sample was withdrawn at different reaction times and

added to 5 mL of a solution containing KI (0.6 M) and HCO_3^- (0.06 M). The Abs of solution at 348 nm was measured after 10 min of reaction and PMS concentration (C_{PMS}, (mM)) was determined as $C_{PMS} = \frac{V_{tot}}{V_{PMS}} \times \frac{Abs_{348\,nm}}{0.5}$. Where V_{PMS} and V_{tot} are the volume of sample (100 µL) and total volume (5.1 mL), 0.5 was the slope of the linear correlation between the PMS concentration and value of Abs at 348 nm.

The Atomic absorption spectroscopy (AAS, PerkinElmer) was employed to determine the concentration of dissolved Mn^{2+} in the aqueous solution. The procedure involved the filtration of the samples through a 0.2 µm PTFE filter and the addition of 2% nitric acid (HNO_3, 65%, Sigma-Aldrich) before detection. Mn^{2+} standard solution for AAS (TraceCERT®, 1000 mg L^{-1} Mn in 2% nitric acid, Sigma-Aldrich) was used for making the calibration curve of Mn^{2+}. The detection wavelength was set at 279.48 nm.

The identification of reactive oxygen species was performed on the electron paramagnetic resonance spectroscopy (EPR, Burker) using 5,5-dimethyl-1-pyrroline N-oxide (DMPO) as the spin trapping agents. Typically, 375 µL of sample was withdrawn and immediately mixed with 125 µL of DMPO (100 mM), then the mixture was transferred into an EPR quartz capillary tube (0.5 mm, 100 mm) for measurement. The EPR spectrometer settings were as follows: modulation frequency, ~100 kHz; microwave frequency, ~9.87 GHz; microwave power, ~6.87 mW; center field, ~352.7 mT; sweep width, 20 mT; sweep time, 30 s; sample g-factors, 2.0; modulation amplitude, 1.0 G.

3. Results and discussion

3.1. Effect of γ-MnOOH and PMS dosage

Preliminary experiments showed that no significant degradation was observed with PMS or γ-MnOOH, while efficient removal was reached when both γ-MnOOH and PMS were used simultaneously (Fig. 1). In this system, BPA was completely removed after 2 h with an initial

pseudo-first order degradation rate (k'BPA) of 0.058 ± 0.001 min^{-1} showing that reactive species (such as $SO_4^{\bullet-}$ and $HO^{\bullet}$) may be generated through the reaction between γ-MnOOH and PMS in solution. Moreover, the adsorption of BPA on γ-MnOOH was negligible (< 3 %) after 3h of reaction.

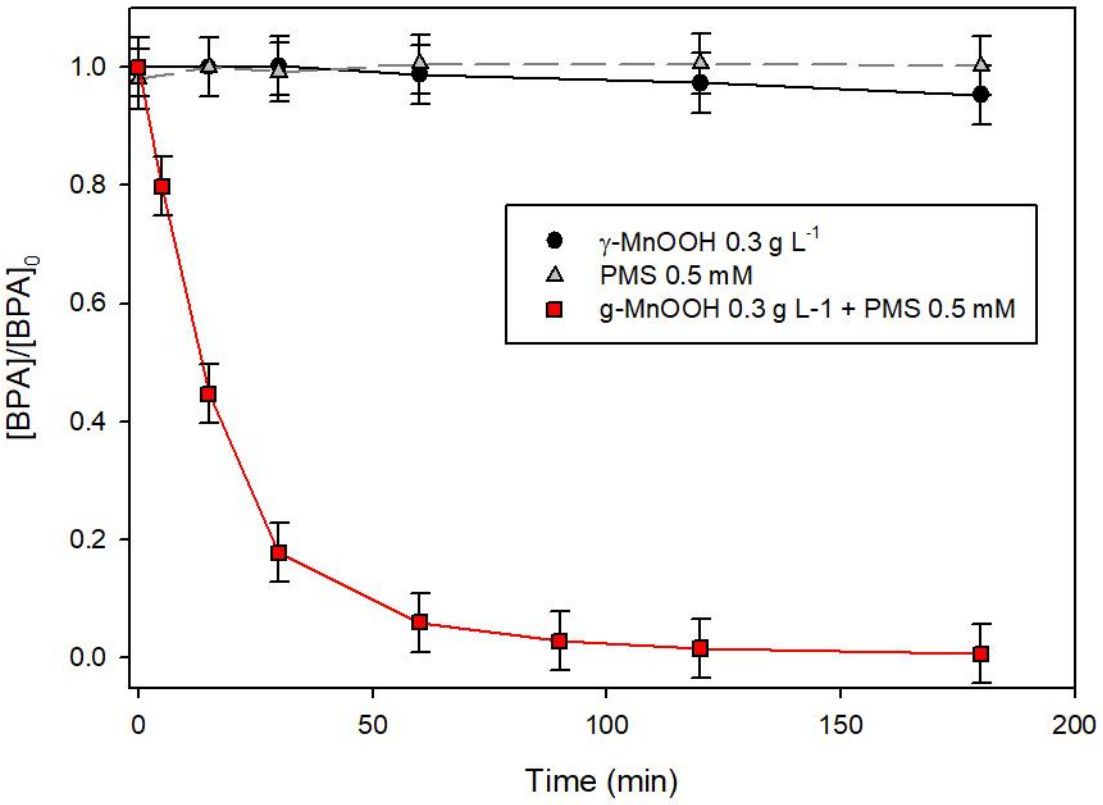

Fig. 1. Degradation of BPA (25 µM) in the presence of γ-MnOOH (0.3 g L^{-1}) and PMS (0.5 mM) at pH 6.5.

When various concentrations of γ-MnOOH were used in the presence of 0.5 mM PMS (Fig. 2A), a different trend can be observed. Increasing the γ-MnOOH concentration up to 0.1 g L^{-1}, faster degradation of BPA was determined and the corresponding kinetic rate constant of BPA degradation (k'_{BPA}) increased up to 0.163 ± 0.001 min^{-1}. At higher γ-MnOOH concentrations, the BPA degradation decreased and almost no degradation was observed using 0.5 g L^{-1} of γ-

MnOOH. Similar trend was observed when different PMS concentrations were used in the presence of 0.1 g L^{-1} of γ-MnOOH (Fig. 2B). From 0 to 2 mM, k'_{BPA} increased almost linearly to 0.719 ± 0.007 min^{-1}, while higher PMS concentrations inhibited the degradation. This behavior suggests that Mn(III)-oxide and PMS would scavenge the generated reactive species when they are used at high concentrations. This behaviour suggests that Mn(III)-oxide and PMS would scavenge the generated reactive species when they are used at high concentrations. This effect can be attributed to the quenching of excessive γ-MnOOH and PMS on the active species(Wang et al., 2017; Zhang et al., 2021). Thus, an optimal concentration of γ-MnOOH (0.1 g/L) and PMS (2 mM) was adopted for the followed study.

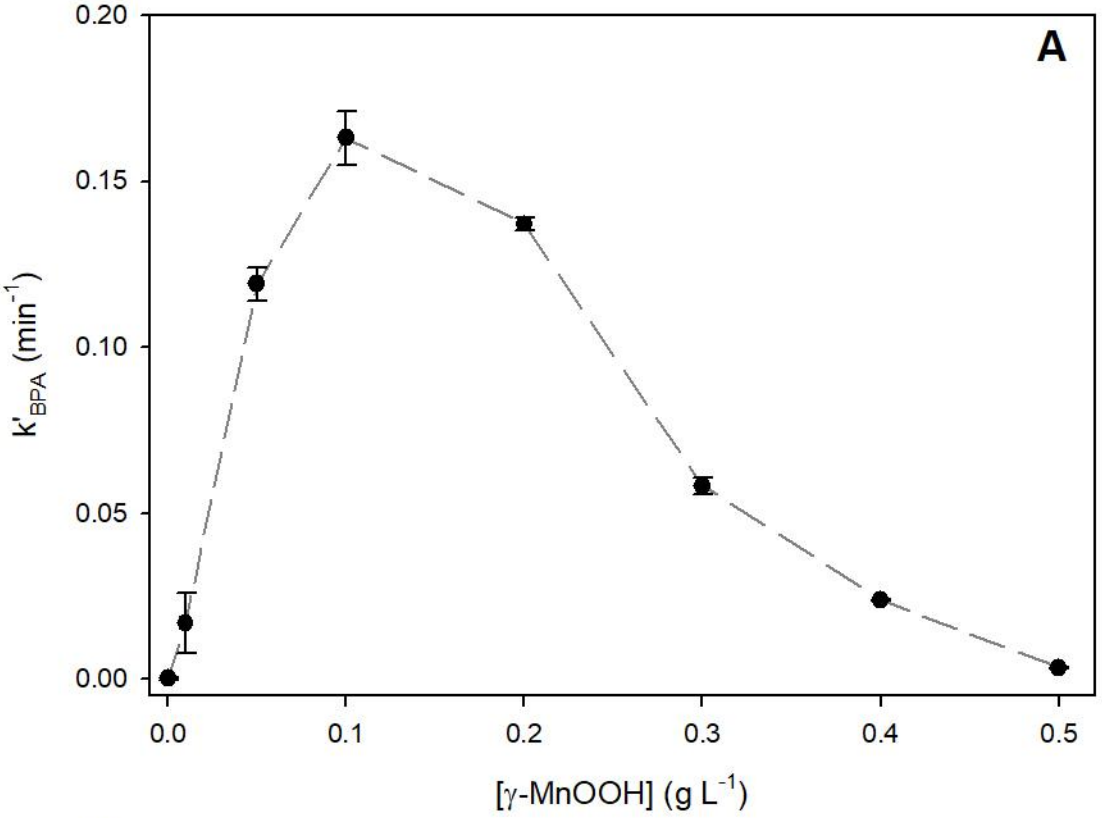
A
0.20
0.15
0.10
0.05
0.00
k'BPA (min-1)
0.0
0.1
0.2
0.3
0.4
0.5
[γ-MnOOH] (g L-1)

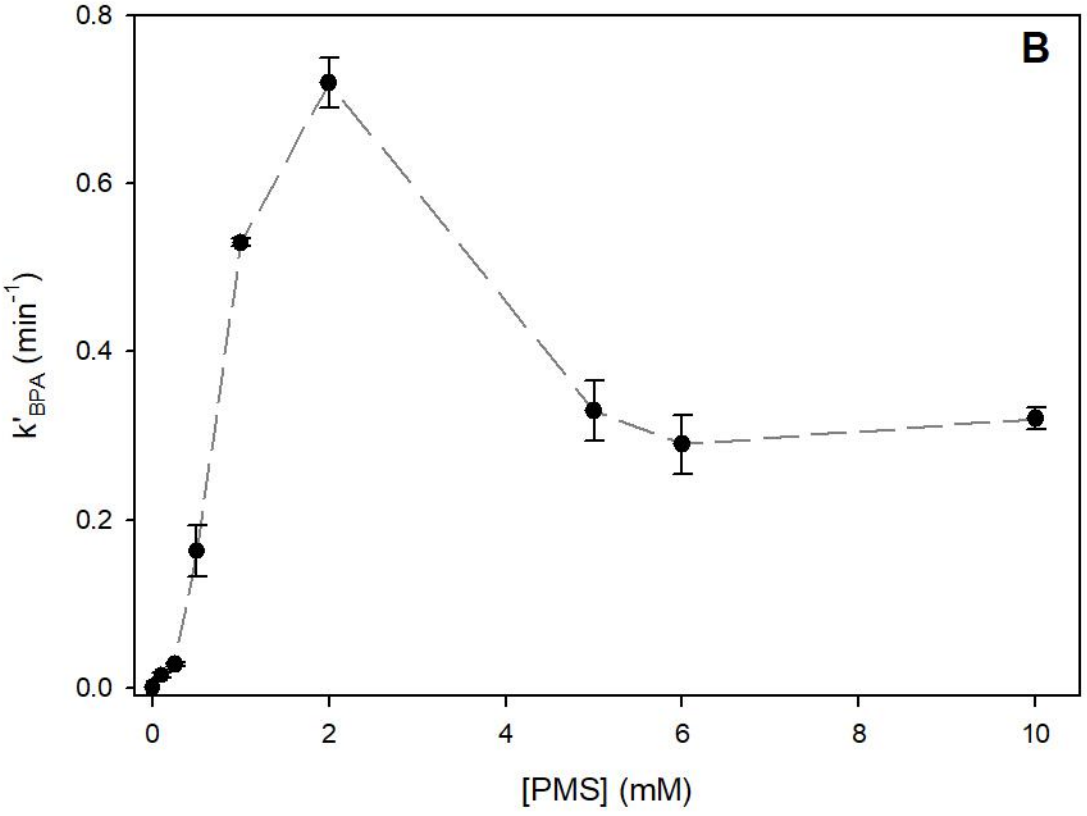
B
0.8
0.6
0.4
0.2
0.0
k'BPA (min-1)
0
2
4
6
8
10
[PMS] (mM)

210

Fig. 2. Pseudo-first order degradation rate of BPA using different γ-MnOOH concentrations in the presence of 0.5 mM of PMS (A) and in the presence of γ-MnOOH (0.1 g L^{-1}) and different PMS concentrations (B). Error bars are determined from the σ-level uncertainty of the data fit used to obtain k'_{BPA}.

3.2. Activation pathway and reactive species formation

In order to verify the generation of reactive species resulted from the activation of γ-MnOOH, the leaching of dissolved Mn^{2+} in γ-MnOOH/PMS system was measured, and the homogenous activation of PMS by Mn^{2+} was evaluated. The total amount of leached and adsorbed Mn^{2+} was determined at around 34 μM after 30 min of reaction. However, a high amount of dissolved Mn^{2+} (100 μM) can only remove about 20% of target compound in 1 h reaction (Fig. S4). Therefore, the removal of BPA was mainly attributed to the heterogeneous activation of PMS by γ-MnOOH.

To identify the reactive species generated in the γ-MnOOH/PMS system, chemical scavenging tests and EPR experiments were conducted. Firstly, the generation of reactive oxidant species was investigated using different chemical quenchers. TBA was used as the $HO^{\bullet}$ scavenger due to its higher selectivity toward $HO^{\bullet}$ ($k_{TBA,HO^{\bullet}} = 6.0 \times 10^8$ M^{-1} s^{-1}) compared to $SO_4^{\bullet-}$ ($k_{TBA,SO_4^{\bullet-}} = 8.4 \times 10^5$ M^{-1} s^{-1}) (Yuan et al., 2019). Theoretically, the addition of 10 mM of TBA can suppress 96% of BPA degradation considering the reaction rate constants of TBA, PMS and BPA with $HO^{\bullet}$ ($k_{PMS,HO^{\bullet}} = 1 \times 10^7$ M^{-1} s^{-1} and $k_{BPA,\ HO^{\bullet}} = 8.6 \times 10^9$ M^{-1} s^{-1}) (Table S2) (W. Huang et al., 2018; Maruthamuthu and Neta, 1977). However, the k'_{BPA} was not inhibited when 10 mM of TBA were added to the solution, indicating that no $HO^{\bullet}$ was generated in the system (Fig. 3). Comparatively, using 10 mM of EtOH can efficiently quench both $HO^{\bullet}$ and $SO_4^{\bullet-}$ radicals ($k_{EtOH,HO^{\bullet}} = 1.9 \times 10^9$ M^{-1} s^{-1} and $k_{EtOH,\ SO_4^{\bullet-}} = 4.3 \times 10^7$ M^{-1} s^{-1}) (Buxton et al., 1988; Clifton and Huie, 1989). The k'_{BPA} decreases to 40 % of the initial value (0.719 min^{-1})

showing that $SO_4^{\bullet-}$ are generated and contributed to the BPA degradation. Further increasing EtOH concentration up to 50 mM, the BPA degradation decreased to 39 %. The generation of reactive radicals were also confirmed by the EPR experiments using DMPO as the complexing agents. Fig. S5 shows one clear seven-peaks signal was formed in the γ-MnOOH/PMS system. This multiplet peaks signal is recognized as the 5,5-dimethyl-2-oxo-pyrroline-1-oxyl (DMPOX) which can be generated by the overoxidizing of DMPO by reactive species such as HSO_5^-, $HO^{\bullet}$ and $SO_4^{\bullet-}$ radicals. Since no $HO^{\bullet}$ was generated in the reaction, and HSO_5^- has low reactivity to oxidize DMPO (X. Yang et al., 2020), the formation of DMPOX can be reasonably attributed to the reactivity of DMPO with $SO_4^{\bullet-}$ radicals.

Furthermore, under the adopted experimental conditions we can estimate that, considering only $SO_4^{\bullet-}$ involved during the degradation system, quenching of 78.5 and 94.8% of BPA degradation should be expected with the addition of 10 and 50 mM of EtOH (Table S2). However, this difference has not been observed in our experiments, which suggest the occurrence of other reactive species un-quenchable by the organic scavengers. Thus, one non-radical mechanism was assumed to be responsible for the degradation of the rest part of BPA. He et al. reported the generation of singlet oxygen ($^1O_2$) in the system of γ-MnOOH/PMS (He et al., 2020). To verify if $^1O_2$ was generated, the degradation of BPA was followed in the presence of 1 mM FFA as $^1O_2$ quencher ($k_{FFA,1_{O_2}}$ = 1.2 × 10^8 M^{-1} s^{-1}) in addition to 50 mM of EtOH (Haag et al., 1984). Since FFA has high reactivity with $HO^{\bullet}$ ($k_{FFA,\ HO^{\bullet}}$ = 1.5 × 10^{10} M^{-1} s^{-1}) (Yang et al., 2018), the simultaneous addition of FFA and EtOH was planned to consume all the possible $HO^{\bullet}$ radicals using EtOH, and then verify the inhibition of BPA degradation caused by FFA addition was only attributed to the generation of $^1O_2$. As reported in Fig. 3, almost no effect was observed with the addition of FFA indicating that $^1O_2$ was not generated.

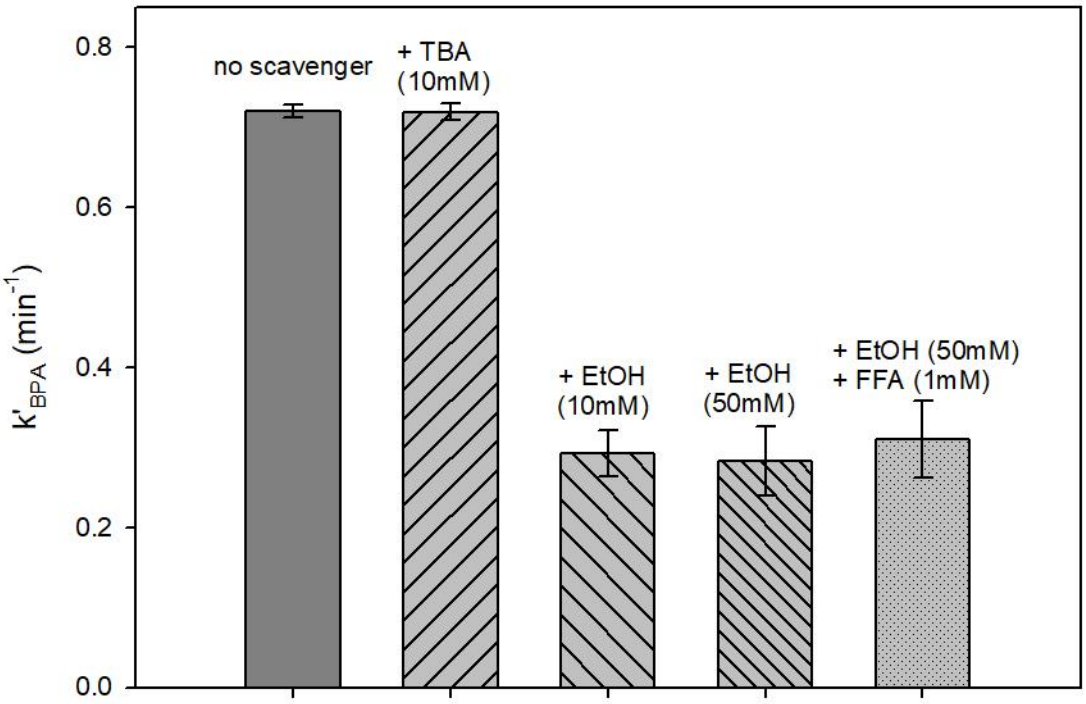

Fig. 3. BPA degradation (k'_{BPA}) in the system γ-MnOOH 0.1 g L^{-1} + PMS 2 mM in the absence and presence of different scavengers at pH 6.5. Error bars are determined from the σ-level uncertainty of the data fit used to obtain k'_{BPA}.

To further shed light on the non-radical mechanism in the γ-MnOOH/PMS system, more attention had been paid to the oxidation states of Mn species changing during the reaction. Since the direct oxidation of the organic compounds by Mn(IV) through electron transfer process has been widely reported (Huang et al., 2019; J. Huang et al., 2018), we can suppose that higher valence state Mn species (e.g. Mn^{IV}) can be formed, and thus contribute to the degradation of BPA. In order to get more insights on the redox process involving Mn species, XPS analysis of γ-MnOOH surfaces was performed during different reaction steps. The chemical oxidation state of Mn in the external layers was determined using the Mn 3s multiplet splitting method and the position and shape of the Mn $2p_{3/2}$ spectra (Fig. 4) (Ardizzone et al.,

1998; Ilton et al., 2016). The peak position and relevant parameters from curve fitting of Mn 3s and Mn $2p_{3/2}$ high resolution spectra are listed in Table 1. The average oxidation state (AOS) of samples was calculated from the % of each Mn species from the fitting of Mn $2p_{3/2}$ spectra and from the binding energy difference of Mn 3s doublet splitting as following: AOS = 8.956 - 1.126 × ΔE [25,26]. Using the multiplets fitting of the Mn $2p_{3/2}$ peaks, the percent contents of Mn(IV), Mn(III) and Mn(II) in the γ-MnOOH sample were 7%, 85% and 8%, respectively and AOS was 2.99. After reaction with PMS, the relative contents of Mn(IV), Mn(III) and Mn(II) changed and Mn(IV) percentage increased to 24.5 consistently with an increase of AOS up to 3.10. In the sample γ-MnOOH + PMS + BPA, Mn(II) percentage increased to 37% while Mn(IV) decreased to 9% with a decrease of AOS down to 2.72. AOS values were consistent with those determined from the fitting of Mn 3s multiplet splitting data (Table 1). The increase of Mn(IV) in the presence of PMS followed by a decrease when BPA was present in solution, suggests that freshly generated Mn(IV) may contribute to the degradation of BPA. Such a process, called metal-based oxidation, was previously indicated as relevant surface-mediated oxidation of organic pollutants in the presence of Mn(IV) oxides (Kamagate et al., 2020). Huang et al. demonstrated the efficient oxidation of BPA by MnO_2 with different structures such as α-, β-, γ-, δ-MnO_2 with and without PMS (Huang et al., 2019; J. Huang et al., 2018). Wang et al. reported the removal of BPA was due to a complex between amorphous MnO_2 and PMS (Wang et al., 2018).

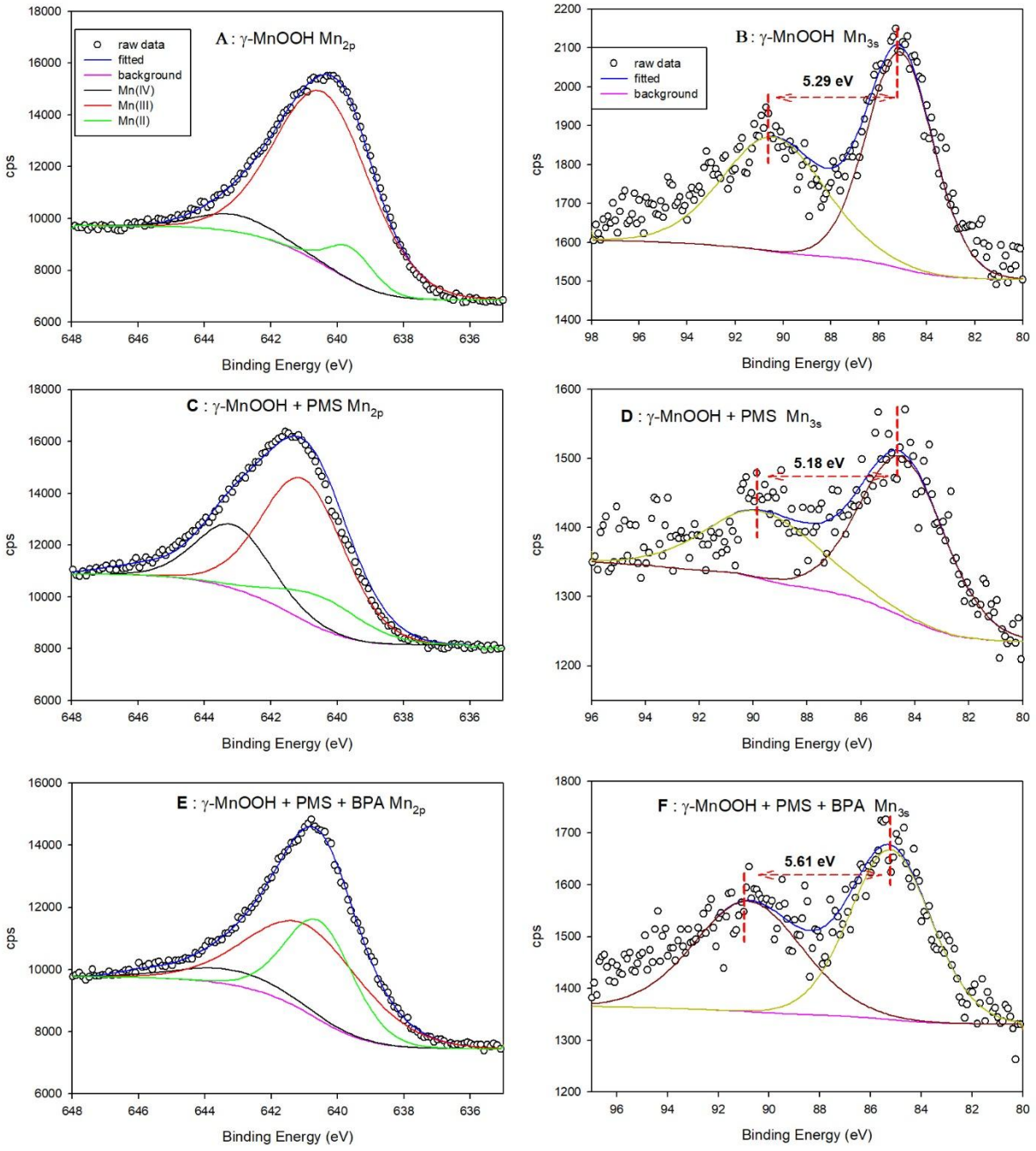

Fig. 4. XPS Mn 2p and Mn 3s spectra of γ-MnOOH (A and B), γ-MnOOH + PMS (C and D) and γ-MnOOH + PMS + BPA (E and F) Initial conditions are [BPA] = 5 μM, [γ-MnOOH] = 0.1 g L^{-1} and [PMS] = 2 mM at pH 6.5.

Table 1. Parameters from curve fitting of Mn 3s and Mn $2p_{3/2}$ XPS spectra and average oxidation state.

	Sample		γ-MnOOH	γ-MnOOH+PMS	γ-MnOOH+PMS+BPA
Mn 2p	**Mn(II)**	BE (eV)	639.60	639.64	640.54
		%	8	14	37
	Mn(III)	BE (eV)	640.41	641.00	640.88
		%	85	61	54
	Mn(IV)	BE (eV)	643.10	642.85	643.18
		%	7	25	9
		AOS	**2.99**	**3.10**	**2.72**
Mn 3s	Multiplet Splitting (eV)		5.29	5.18	5.61
		AOS	**3.00**	**3.12**	**2.64**

Collectively, quenching experiments and XPS analysis suggest that the first electron transfer reaction occurring between ≡Mn(III) and PMS on the surface of oxide led to the formation of ≡Mn(IV) and $SO_4^{\bullet-}$ (R1). $SO_4^{\bullet-}$ can oxidize BPA (R4) (Table S2) while Mn(IV) can further react with PMS leading to the formation of ≡Mn(III) and $SO_5^{\bullet-}$ (R2) or directly with BPA (R3). The involvement of $SO_5^{\bullet-}$ during the BPA degradation (R5) is reasonably considered less relevant due to the typical second-order rate constants between $SO_5^{\bullet-}$ and organic molecules (10^4 - 10^6 M^{-1} s^{-1}) (Huie and Neta, 1985).

$$\equiv Mn(III) + HSO_5^- \rightarrow \equiv Mn(IV) + HO^- + SO_4^{\bullet-} \quad \text{(R1)}$$

$$\equiv Mn(IV) + HSO_5^- \rightarrow \equiv Mn(III) + SO_5^{\bullet-} + H^+ \quad \text{(R2)}$$

$$\equiv Mn(IV) + BPA \rightarrow \equiv Mn(II/III) + BPA_{ox} \quad \text{(R3)}$$

$$SO_4^{\bullet-} + BPA \rightarrow SO_4^{2-} + BPA_{ox} \quad \text{(R4)}$$

$$SO_5^{\bullet-} + BPA \rightarrow SO_5^{2-} + BPA_{ox} \quad \text{(R5)}$$

3.3. Degradation and mineralization of BPA, E2 and EE2

Degradation and mineralization efficiencies of γ-MnOOH/PMS system were tested on BPA, E2 and EE2 mixing solution at pH 6.5. In Fig. 5, the degradation of three EDCs (5 µM each) and PMS (2 mM) consumption were followed during the reaction time in the presence of γ-MnOOH (0.1 g L^{-1}). Despite no degradation in the presence of γ-MnOOH alone and less than 10 % after 2 hours in the presence of PMS alone (Fig. S6), almost complete degradation of three pollutants can be observed after 30 min. Degradation of BPA, E2 and EE2 follows a mono-exponential decay and after 30 min of reaction, ~ 100 µM of PMS were consumed. We can then estimate an efficiency of degradation system considering the stoichiometric efficiency value (η) that is calculated as the ratio between degraded EDCs vs consumed PMS ($\eta = \frac{\Delta[EDCs]}{\Delta[PMS]}$). In the presence of 0.1 g L^{-1} γ-MnOOH and 2 mM of PMS a value of η = 15% was determined at pH 6.5.

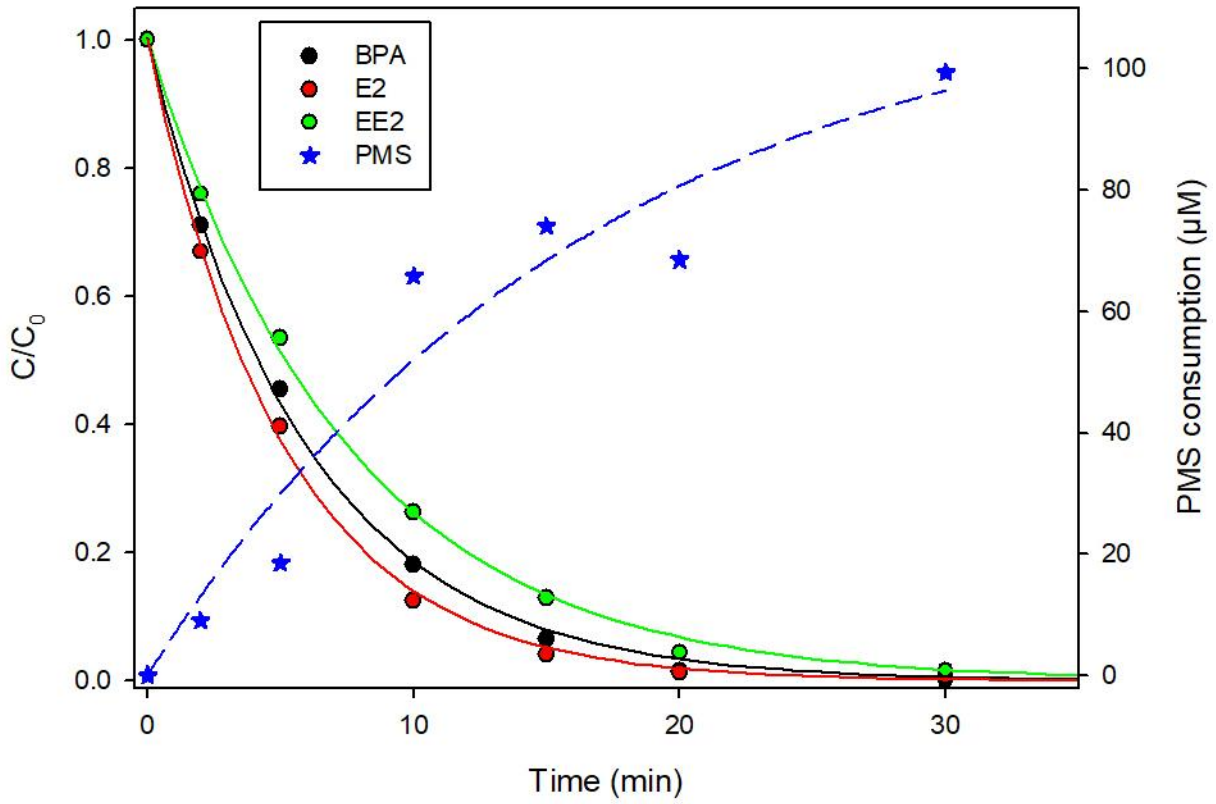

Fig. 5. Degradation of BPA, E2 and EE2 in the system γ-MnOOH/PMS. The solid lines show the fit of data using a mono-exponential decay function. Blue points show the PMS consumption during the reaction. Initial conditions are [BPA] = [E2] = [EE2] = 5 μM, [γ-MnOOH] = 0.1 g L^{-1} and [PMS] = 2 mM at pH 6.5.

The reuse of γ-MnOOH is an important parameter with regard to the possible application in water treatment processes. For this purpose, the degradation efficiency (DE) for each EDCs after 30 min of reaction was tested for 3 cycles. For the recycling experiments, the solution containing mainly soluble products (PMS and EDCs degradation products) was completely removed from the reactor and a fresh solution containing PMS and EDCs at initial concentration was added again into the reactor containing γ-MnOOH. As shown in Fig. 6, after

three cycles of reuse, a reduction of EDCs degradation efficiency of about 20 % was observed indicating a good reusability of the oxidative system for EDCs removal. This effect can be explained considering the generation of $\equiv Mn(II)$ (R3) and slower formation of $\equiv Mn(III)$ through PMS reactivation (R6) (Gao et al., 2021).

$$\equiv Mn(II) + HSO_5^- \rightarrow \equiv Mn(III) + SO_4^{\bullet -} + HO^- \quad \text{(R6)}$$

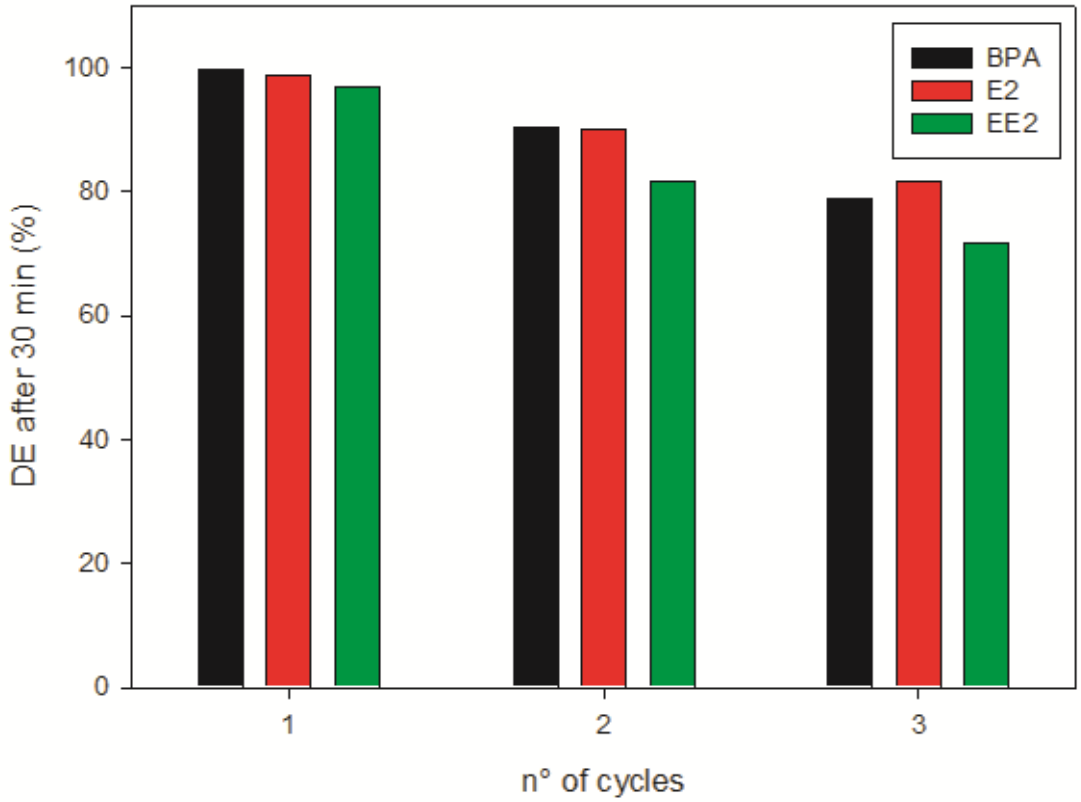

Fig. 6. Reusability of γ-MnOOH over 3 cycles. Experimental conditions are: [γ-MnOOH] = 0.1 g L^{-1}, [PMS] = 2 mM, [BPA] = [E2] = [EE2] = 5µM and pH = 6.5.

3.4. Effect of inorganic ions

Inorganic anions are commonly detected in natural waters and they could affect the radical-mediated degradation efficiency of organic pollutants. In the γ-MnOOH / PMS system, the effect of chloride (Cl^-), bicarbonate (HCO_3^-), nitrite (NO_2^-) and nitrate (NO_3^-) anions was

362 investigated and BPA, E2, and EE2 degradations were followed using 0.1 g L^{-1} of γ-MnOOH
363 and 2 mM of PMS.
364 As illustrated in Fig. 7A, increasing the concentration of Cl^- from 0 to 5 mM, the BPA, E2, and
365 EE2 degradation rates slightly increased indicating a positive effect of Cl^- on the oxidation
366 system. The results are in agreement with previous studies which indicated that improvement of
367 organic pollutants degradation efficiency in the presence of Cl^- was attributed to the generation
368 of reactive chlorine species such as $Cl^•$ and HOCl (R7 to R9) (Wang and Wang, 2021). In fact,
369 despite a different reactivity constant between $Cl^•$ and $Cl_2^{•-}$ with organic compounds ($k_{Cl^•}$ = 10^9
370 - 10^{10} M^{-1} s^{-1}, $k_{Cl_2^{•-}}$ = 10^7-10^8 M^{-1} s^{-1}), their lower reactivity was partially counterbalanced by
371 direct activation occurring in the presence of PMS leading to the formation of oxidant species
372 such as HOCl as observed at high Cl^- concentration in absence of γ-MnOOH (R9) (Fig. S6)
373 (Lente et al., 2009).

374 $SO_4^{•-} + Cl^- \rightarrow SO_4^{2-} + Cl^•$ (R7)

375 $Cl^• + Cl^- \rightarrow Cl_2^{•-}$ (R8)

376 $HSO_5^- + Cl^- \rightarrow SO_4^{2-} + HOCl$ (R9)

377 Bicarbonate ions (HCO_3^-) are generally considered as interfering species during oxidative
378 processes based on radical species generation due to their reactivity with radicals and
379 generation of less oxidative species such as $CO_3^{•-}$ (Buxton et al., 1988; Clifton and Huie, 1989).
380 However, a negligible impact on the EDCs degradation was observed with the addition of
381 HCO_3^- (Fig. 7B). Such effect can be explained considering that the inhibition effect on the
382 sulfate radical reactivity (R10-R11) is counterbalanced by the direct activation of HCO_3^- by
383 PMS leading to the formation of HCO_4^- as reported in Fig. S7 (R12) (Wang and Wang, 2021).

384 $SO_4^{•-} + CO_3^{2-} \rightarrow SO_4^{2-} + CO_3^{•-}$ (R10)

385 $SO_4^{•-} + HCO_3^- \rightarrow SO_4^{2-} + CO_3^{•-} + H^+$ (R11)

386 $HSO_5^- + HCO_3^- \rightarrow SO_4^{2-} + HCO_4^- + H^+$ (R12)

The effect of nitrogen anions (NO_2^- and NO_3^-) on BPA, E2 and EE2 degradation were investigated, individually. As shown in Fig. S8, no effect of both NO_2^- and NO_3^- on the degradation of the three EDCs was observed.

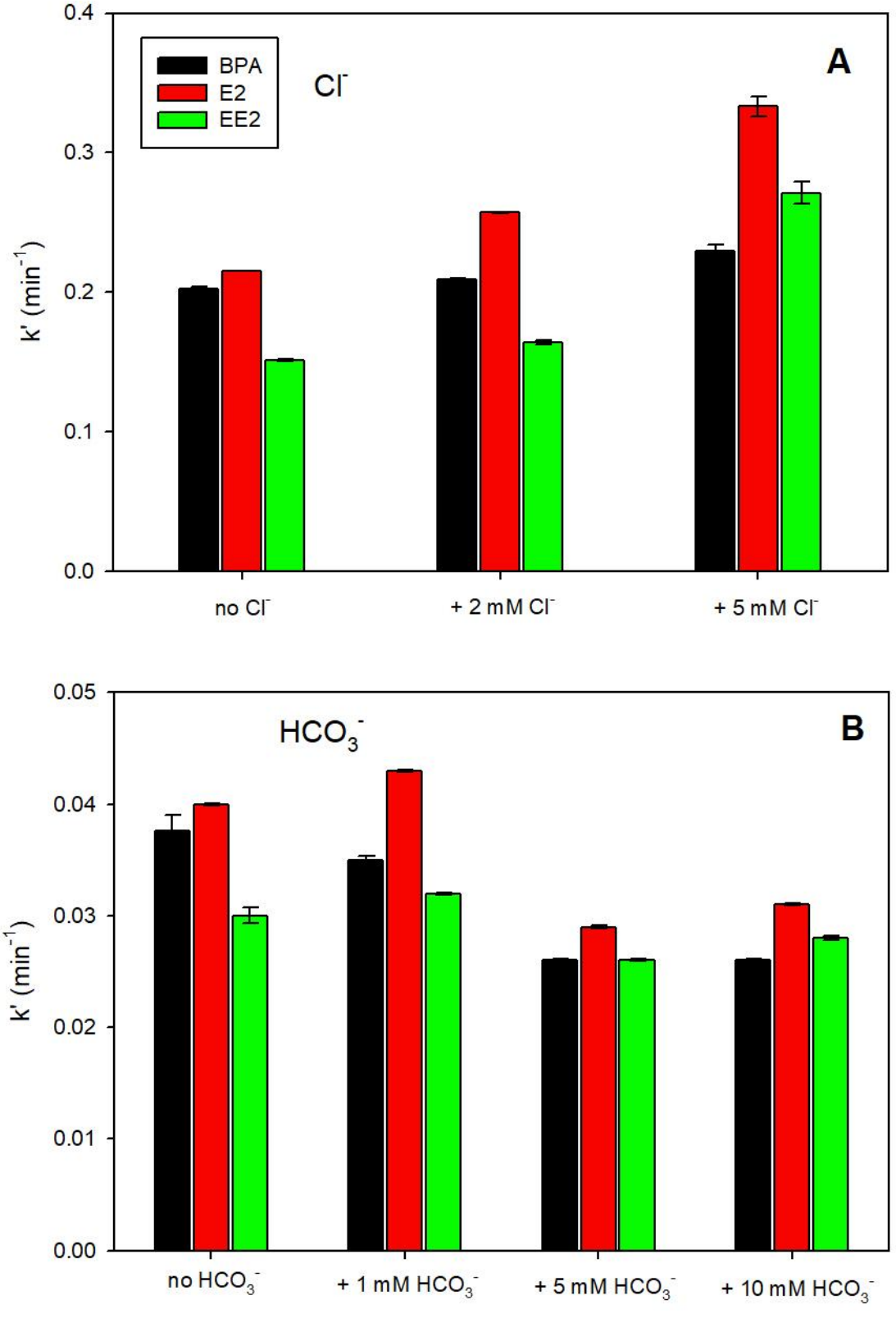

Fig. 7. Effect of chloride ions (Cl^-) (**A**) and bicarbonate ions (HCO_3^-) (**B**) on the degradation of BPA, E2, and EE2 using γ-MnOOH/PMS system. Experimental conditions are: [γ-MnOOH] = 0.1 g L^{-1}, [PMS] = 2 mM, [BPA] = [E2] = [EE2] = 5μM, pH = 6.5 (for Cl^-) and pH = 8.0 (for

396 HCO_3^-). Error bars are determined from the σ-level uncertainty of the data fit used to obtain k'
397 of estrogens.
398
399 *3.5. Efficiency in the real water matrix*
400 To evaluate the efficiency of γ-MnOOH/PMS system in realistic conditions, the treatment of
401 three EDCs in filtered sewage treatment plant water (STPW) was conducted. The initial TOC
402 was determined to be 10.8 mgC L^{-1} (in which 2.8 mgC L^{-1} come from the addition of 3 EDCs).
403 As expected, the removal rates and efficiencies of EDCs and TOC in STP water were slower in
404 comparison with results in milli-Q water (Fig. 8). This effect can be attributed to the organic
405 matter and inorganic anions present in STP water, which can compete with degradation EDCs
406 during the γ-MnOOH/PMS process. It is interesting to notice that EDCs initial degradation in
407 STP water is lower during the first 15 min and rapidly increases to almost complete removal
408 after 35-40 min. 18 % of TOC removal was also observed after 30 min of reaction and TOC
409 removal continues after EDCs degradation with a rate of 0.067 ± 0.007 mgC min^{-1}.

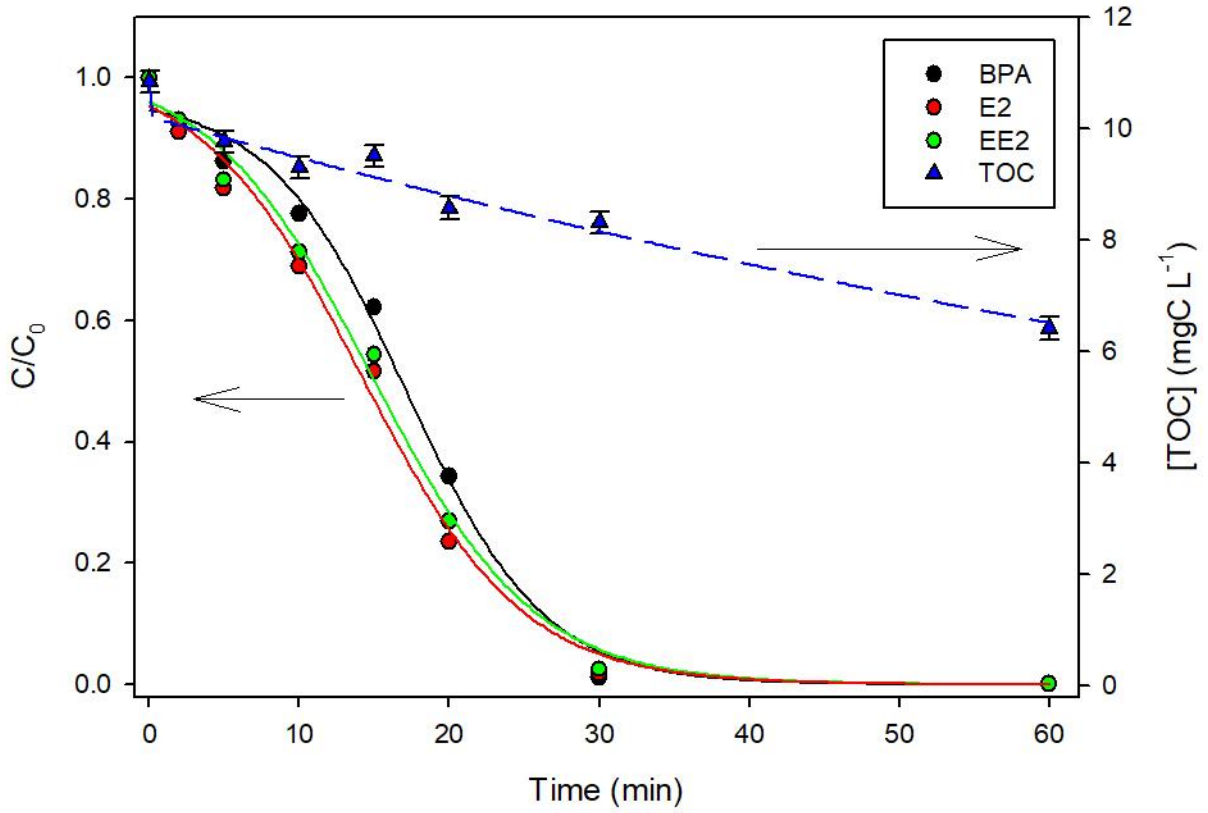

Fig. 8. BPA, E2 and EE2 degradation by γ-MnOOH/PMS system in STPW and TOC removal. Experimental conditions are: [γ-MnOOH] = 0.1 g L^{-1}, [PMS] = 2 mM, [BPA] = [E2] = [EE2] = 5μM, and pH = 6.5. Error bars on TOC analysis was 0.2 mgC L^{-1}.

4. Conclusion

In this work, the degradation of three estrogens: BPA, E2 and EE2 was performed using manganite (γ-MnOOH) in the presence of peroxymonosulfate ions (PMS). The rapid degradation in water was attributed to the generation of sulfate radical and the direct oxidation mediated by Mn(IV). In fact, about 60% of estrogens degradation was attributed to the generation of sulfate radical, while ~ 40 % to the direct oxidation mediated by Mn(IV). The effect of inorganic ions at environmentally relevant concentrations showed only limited inhibition effect on EDCs degradation in ultrapure water and real sewage treatment plant water, indicating that the γ-MnOOH/PMS system can be applied for real wastewater treatment. The

Mn(III)/(IV) cycle represents the main reaction step leading to the formation of sulfate radical but also mediated Mn(IV) species have high oxidation ability toward the removal of selected pollutants. These results have strong implications for the development of Mn-mediated oxidation processes in wastewater remediation technologies.

Acknowledgements

We gratefully acknowledge the Chinese Scholarship Council of PR China for providing financial support for Daqing Jia. This work was supported by the Institut Universitaire de France, the Region Council of Auvergne Rhône-Alpes and the CNRS.

References

Abida, O., Mailhot, G., Litter, M., Bolte, M., 2006. Impact of iron-complex (Fe(III)–NTA) on photoinduced degradation of 4-chlorophenol in aqueous solution. Photochem. Photobiol. Sci. 5, 395–402. https://doi.org/10.1039/B518211E

Adeel, M., Song, X., Wang, Y., Francis, D., Yang, Y., 2017. Environmental impact of estrogens on human, animal and plant life: A critical review. Environment International 99, 107–119. https://doi.org/10.1016/j.envint.2016.12.010

Ardizzone, S., Bianchi, C.L., Tirelli, D., 1998. Mn3O4 and γ-MnOOH powders, preparation, phase composition and XPS characterisation. Colloids and Surfaces A: Physicochemical and Engineering Aspects 134, 305–312. https://doi.org/10.1016/S0927-7757(97)00219-7

Buxton, G.V., Greenstock, C.L., Helman, W.P., Ross, A.B., 1988. Critical review of rate constants for reactions of hydrated electrons, hydrogen atoms and hydroxyl radicals (· OH/· O− in aqueous solution. Journal of physical and chemical reference data 17, 513–886.

Chaves, F.P., Gomes, G., Della-Flora, A., Dallegrave, A., Sirtori, C., Saggioro, E.M., Bila, D.M., 2020. Comparative endocrine disrupting compound removal from real wastewater by UV/Cl and UV/H2O2: Effect of pH, estrogenic activity, transformation products and toxicity. Science of The Total Environment 746, 141041. https://doi.org/10.1016/j.scitotenv.2020.141041

Clifton, C.L., Huie, R.E., 1989. Rate constants for hydrogen abstraction reactions of the sulfate radical, SO4−. Alcohols. International Journal of Chemical Kinetics 21, 677–687. https://doi.org/10.1002/kin.550210807

Gabet, A., Métivier, H., de Brauer, C., Mailhot, G., Brigante, M., 2021. Hydrogen peroxide and persulfate activation using UVA-UVB radiation: Degradation of estrogenic compounds and application in sewage treatment plant waters. Journal of Hazardous Materials 405, 124693. https://doi.org/10.1016/j.jhazmat.2020.124693

Gao, Y., Zhou, Y., Pang, S.-Y., Jiang, J., Shen, Y.-M., Song, Y., Duan, J.-B., Guo, Q., 2021. Enhanced peroxymonosulfate activation via complexed Mn(II): A novel non-radical oxidation mechanism involving manganese intermediates. Water Research 193, 116856. https://doi.org/10.1016/j.watres.2021.116856

Gligorovski, S., Strekowski, R., Barbati, S., Vione, D., 2015. Environmental Implications of Hydroxyl Radicals (•OH). Chem. Rev. 115, 13051–13092. https://doi.org/10.1021/cr500310b

Gmurek, M., Olak-Kucharczyk, M., Ledakowicz, S., 2017. Photochemical decomposition of endocrine disrupting compounds – A review. Chemical Engineering Journal, Intensification of Photocatalytic Processes for Niche Applications in the Area of Water, Wastewater and Air Treatment 310, 437–456. https://doi.org/10.1016/j.cej.2016.05.014

Haag, W.R., Hoigne´, J., Gassman, E., Braun, A., 1984. Singlet oxygen in surface waters — Part I: Furfuryl alcohol as a trapping agent. Chemosphere 13, 631–640. https://doi.org/10.1016/0045-6535(84)90199-1

Havens, S.M., Hedman, C.J., Hemming, J.D.C., Mieritz, M.G., Shafer, M.M., Schauer, J.J., 2020. Occurrence of estrogens, androgens and progestogens and estrogenic activity in surface water runoff from beef and dairy manure amended crop fields. Science of The Total Environment 710, 136247. https://doi.org/10.1016/j.scitotenv.2019.136247

He, D., Li, Y., Lyu, C., Song, L., Feng, W., Zhang, S., 2020. New insights into MnOOH/peroxymonosulfate system for catalytic oxidation of 2,4-dichlorophenol: Morphology dependence and mechanisms. Chemosphere 255, 126961. https://doi.org/10.1016/j.chemosphere.2020.126961

Huang, J., Dai, Y., Singewald, K., Liu, C.-C., Saxena, S., Zhang, H., 2019. Effects of MnO2 of different structures on activation of peroxymonosulfate for bisphenol A degradation under acidic conditions. Chemical Engineering Journal 370, 906–915. https://doi.org/10.1016/j.cej.2019.03.238

Huang, J., Zhong, S., Dai, Y., Liu, C.-C., Zhang, H., 2018. Effect of MnO_2 Phase Structure on the Oxidative Reactivity toward Bisphenol A Degradation. Environ. Sci. Technol. 52, 11309–11318. https://doi.org/10.1021/acs.est.8b03383

Huang, W., Bianco, A., Brigante, M., Mailhot, G., 2018. UVA-UVB activation of hydrogen peroxide and persulfate for advanced oxidation processes: Efficiency, mechanism and effect of various water constituents. Journal of hazardous materials 347, 279–287.

Huang, W., Brigante, M., Wu, F., Mousty, C., Hanna, K., Mailhot, G., 2013. Assessment of the Fe(III)–EDDS Complex in Fenton-Like Processes: From the Radical Formation to the Degradation of Bisphenol A. Environ. Sci. Technol. 47, 1952–1959. https://doi.org/10.1021/es304502y

Huie, R.E., Neta, P., 1985. One-electron redox reactions in aqueous solutions of sulfite with hydroquinone and other hydroxyphenols. J. Phys. Chem. 89, 3918–3921. https://doi.org/10.1021/j100264a032

Ilton, E.S., Post, J.E., Heaney, P.J., Ling, F.T., Kerisit, S.N., 2016. XPS determination of Mn oxidation states in Mn (hydr)oxides. Applied Surface Science (1985) 366, 475–485. https://doi.org/10.1016/j.apsusc.2015.12.159

Kamagate, M., Pasturel, M., Brigante, M., Hanna, K., 2020. Mineralization Enhancement of Pharmaceutical Contaminants by Radical-Based Oxidation Promoted by Oxide-Bound Metal Ions. Environmental Science and Technology 54, 476–485. https://doi.org/10.1021/acs.est.9b04542

Kusic, H., Peternel, I., Ukic, S., Koprivanac, N., Bolanca, T., Papic, S., Bozic, A.L., 2011. Modeling of iron activated persulfate oxidation treating reactive azo dye in water matrix. Chemical Engineering Journal 172, 109–121. https://doi.org/10.1016/j.cej.2011.05.076

Lei, K., Lin, C.-Y., Zhu, Y., Chen, W., Pan, H.-Y., Sun, Z., Sweetman, A., Zhang, Q., He, M.-C., 2020. Estrogens in municipal wastewater and receiving waters in the Beijing-Tianjin-Hebei region, China: Occurrence and risk assessment of mixtures. Journal of Hazardous Materials 389, 121891. https://doi.org/10.1016/j.jhazmat.2019.121891

Lente, G., Kalmár, J., Baranyai, Z., Kun, A., Kék, I., Bajusz, D., Takács, M., Veres, L., Fábián, I., 2009. One- Versus Two-Electron Oxidation with Peroxomonosulfate Ion: Reactions with Iron(II), Vanadium(IV), Halide Ions, and Photoreaction with Cerium(III). Inorg. Chem. 48, 1763–1773. https://doi.org/10.1021/ic801569k

Li, Y., Liu, L.-D., Liu, L., Liu, Y., Zhang, H.-W., Han, X., 2016. Efficient oxidation of phenol by persulfate using manganite as a catalyst. Journal of Molecular Catalysis A: Chemical 411, 264–271. https://doi.org/10.1016/j.molcata.2015.10.036

Maruthamuthu, P., Neta, P., 1977. Radiolytic chain decomposition of peroxomonophosphoric and peroxomonosulfuric acids. Journal of Physical Chemistry 81, 937–940.

Saputra, E., Muhammad, S., Sun, H., Ang, H.-M., Tadé, M.O., Wang, S., 2014. Shape-controlled activation of peroxymonosulfate by single crystal α-Mn2O3 for catalytic phenol degradation in aqueous solution. Applied Catalysis B: Environmental 154–155, 246–251. https://doi.org/10.1016/j.apcatb.2014.02.026

Vilela, C.L.S., Bassin, J.P., Peixoto, R.S., 2018. Water contamination by endocrine disruptors: Impacts, microbiological aspects and trends for environmental protection. Environmental Pollution 235, 546–559. https://doi.org/10.1016/j.envpol.2017.12.098

Wacławek, S., Grübel, K., Cernik, M., 2015. Simple spectrophotometric determination of monopersulfate. Spectrochimica Acta Part A Molecular and Biomolecular Spectroscopy 149. https://doi.org/10.1016/j.saa.2015.05.029

Wang, J., Wang, S., 2021. Effect of inorganic anions on the performance of advanced oxidation processes for degradation of organic contaminants. Chemical Engineering Journal 411, 128392. https://doi.org/10.1016/j.cej.2020.128392

Wang, J., Wang, S., 2018. Activation of persulfate (PS) and peroxymonosulfate (PMS) and application for the degradation of emerging contaminants. Chemical Engineering Journal 334, 1502–1517. https://doi.org/10.1016/j.cej.2017.11.059

Wang, L., Jiang, J., Pang, S.-Y., Zhou, Y., Li, J., Sun, S., Gao, Y., Jiang, C., 2018. Oxidation of bisphenol A by nonradical activation of peroxymonosulfate in the presence of amorphous manganese dioxide. Chemical Engineering Journal 352, 1004–1013. https://doi.org/10.1016/j.cej.2018.07.103

Wang, N., Jia, D., Jin, Y., Sun, S.-P., Ke, Q., 2017. Enhanced Fenton-like degradation of TCE in sand suspensions with magnetite by NTA/EDTA at circumneutral pH. Environ Sci Pollut Res 24, 17598–17605. https://doi.org/10.1007/s11356-017-9387-5

Wang, Y., Indrawirawan, S., Duan, X., Sun, H., Ang, H.M., Tadé, M.O., Wang, S., 2015. New insights into heterogeneous generation and evolution processes of sulfate radicals for phenol degradation over one-dimensional α-MnO2 nanostructures. Chemical Engineering Journal 266, 12–20. https://doi.org/10.1016/j.cej.2014.12.066

Xiong, Z., Jiang, Y., Wu, Z., Yao, G., Lai, B., 2020. Synthesis strategies and emerging mechanisms of metal-organic frameworks for sulfate radical-based advanced oxidation process: A review. Chemical Engineering Journal 127863. https://doi.org/10.1016/j.cej.2020.127863

Xu, X., Zhang, Y., Zhou, S., Huang, R., Huang, S., Kuang, H., Zeng, X., Zhao, S., 2021. Activation of persulfate by MnOOH: Degradation of organic compounds by nonradical mechanism. Chemosphere 272, 129629. https://doi.org/10.1016/j.chemosphere.2021.129629

Yang, C., Song, G., Lim, W., 2020. Effects of endocrine disrupting chemicals in pigs. Environmental Pollution 263, 114505. https://doi.org/10.1016/j.envpol.2020.114505

Yang, X., Wang, X., Li, Y., Wu, Z., Wu, W.D., Chen, X.D., Sun, J., Sun, S.-P., Wang, Z., 2020. A Bimetallic Fe–Mn Oxide-Activated Oxone for In Situ Chemical Oxidation (ISCO) of Trichloroethylene in Groundwater: Efficiency, Sustained Activity, and Mechanism Investigation. Environ. Sci. Technol. 54, 3714–3724. https://doi.org/10.1021/acs.est.0c00151

Yang, Y., Banerjee, G., Brudvig, G.W., Kim, J.-H., Pignatello, J.J., 2018. Oxidation of Organic Compounds in Water by Unactivated Peroxymonosulfate. Environ. Sci. Technol. 52, 5911–5919. https://doi.org/10.1021/acs.est.8b00735

Yu, C., Boily, J.-F., Shchukarev, A., Drake, H., Song, Z., Hogmalm, K.J., Åström, M.E., 2018. A cryogenic XPS study of Ce fixation on nanosized manganite and vernadite: Interfacial reactions and effects of fulvic acid complexation. Chemical Geology 483, 304–311. https://doi.org/10.1016/j.chemgeo.2018.02.033

Yuan, Y., Luo, T., Xu, J., Li, J., Wu, F., Brigante, M., Mailhot, G., 2019. Enhanced oxidation of aniline using Fe(III)-S(IV) system: Role of different oxysulfur radicals. Chemical Engineering Journal 362, 183–189. https://doi.org/10.1016/j.cej.2019.01.010

Zhang, H., Wang, X., Li, Y., Zuo, K., Lyu, C., 2021. A novel MnOOH coated nylon membrane for efficient removal of 2,4-dichlorophenol through peroxymonosulfate activation. Journal of Hazardous Materials 414, 125526. https://doi.org/10.1016/j.jhazmat.2021.125526

Zhao, Yan, Zhao, Yongsheng, Zhou, R., Mao, Y., Tang, W., Ren, H., 2016. Insights into the degradation of 2,4-dichlorophenol in aqueous solution by α-MnO_2 nanowire activated persulfate: catalytic performance and kinetic modeling. RSC Adv. 6, 35441–35448. https://doi.org/10.1039/C6RA00008H

Zhou, X., Yang, Z., Luo, Z., Li, H., Chen, G., 2019. Endocrine disrupting chemicals in wild freshwater fishes: Species, tissues, sizes and human health risks. Environmental Pollution 244, 462–468. https://doi.org/10.1016/j.envpol.2018.10.026